# Accepted Manuscript

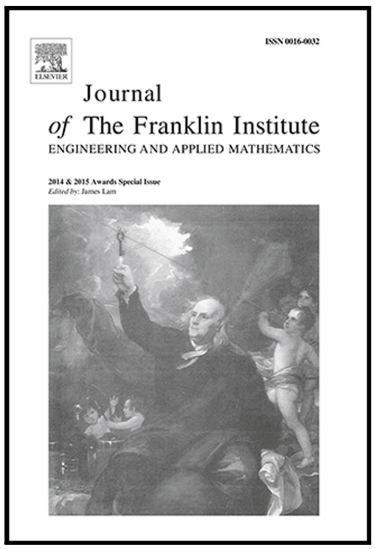


A Decentralized Control Method for Frequency Restoration and Accurate Reactive Power Sharing in Islanded Microgrids

Zhanqiang Zhang , Chunxia Dou , Dong Yue , Bo Zhang , Wei Luo

PII: S0016-0032(18)30598-2
DOI: https://doi.org/10.1016/j.jfranklin.2018.09.024
Reference: FI 3634

To appear in: *Journal of the Franklin Institute*

Received date: 3 May 2018
Revised date: 14 July 2018
Accepted date: 4 September 2018

Please cite this article as: Zhanqiang Zhang , Chunxia Dou , Dong Yue , Bo Zhang , Wei Luo , A Decentralized Control Method for Frequency Restoration and Accurate Reactive Power Sharing in Islanded Microgrids, *Journal of the Franklin Institute* (2018), doi: https://doi.org/10.1016/j.jfranklin.2018.09.024

# A Decentralized Control Method for Frequency Restoration and Accurate Reactive Power Sharing in Islanded Microgrids

Zhanqiang Zhang[1], Chunxia Dou[1,2*], Dong Yue[2*], Bo Zhang[1], Wei Luo[1]
[1] *Institute of Electrical Engineering, Yanshan University, Qinhuangdao 066004, P. R. China*
[2] *Institute of Advanced Technology, Nanjing University of Posts and Telecommunications, Nanjing 210023, P. R. China*
[*]Corresponding authors: cxdou@ysu.edu.cn (C. Dou), medongy@vip.163.com (D. Yue).

**Abstract:** To achieve the frequency restoration (FR) and accurate reactive power sharing (RPS) in islanded microgrids (MGs), an improved P-f droop control is proposed. Firstly, the inverter impedance, whose value is set by the virtual impedance method, is used to minimize the impact of line resistance on powers coupling and RPS. Then, in order to restore the frequency of distributed generations (DGs) to the rated value, the reference is changed for compensating the frequency deviation (FD) caused by loads change. And the fast FR rate is achieved under a large constant *k*. Besides, in order to eliminate the inaccuracy of RPS caused by voltages difference (VD), the line voltage drop (LVD) is used to compensate the voltage droop characteristics. The use of voltage feedback ensures that the obtained voltage is desired after the LVD compensation. Finally, the simulation in RT-LAB indicates the effectiveness of proposed method in an islanded MG model.
**Keywords:** Frequency restoration, reactive power sharing, reference change, line voltage drop compensation, voltage feedback.

## 1. Introduction

MG, which is composed of DG unit, storage battery and loads, can provide the reliable electricity to critical loads by integrating large amounts of DGs [1, 2]. Based on the characteristics of synchronous generator, the P-f droop control has been proposed for the islanded MGs, and it can be used to control DGs in a decentralized peer-peer control manner. Because the resistive transmission line is predominant in the low-voltage (LV) MGs, there will be the problem of powers coupling when the P-f droop control is used [3, 4]. So, the transient response and steady-state performance of MG may be deteriorated [5]. Through increasing the additional inductor to system lines, the virtual impedance method is used to decouple powers for enhancing the power sharing ability and control stability, which makes the P-f control applicable to the LV MG [6]. Since the output active power of DG is proportional to frequency, a challenge of the basic frequency droop control is the deviation from the rated value under the load change [7]. The FD may deteriorate the power quality, decrease the dynamic performance, and shorten the service life in damaging loads [6, 8, 9]. Besides, the slight deviation also exists in voltage due to the LVD between DG and bus. If lines impedances are mismatched, the different LVDs will result in the VD. Thus, the reactive power can't be shared proportionally in accordance with the ratio of droop coefficients among DGs [10]. The inaccurate RPS may disturb the normal powers allocation of loads, reduce the efficiency of electricity supply and the stability of DGs' output powers.

Two main control architectures for FR and accurate RPS are the centralized/distributed coordinate and decentralized. The former requires the communication network to support the necessary interaction between DGs. Some common centralized/distributed coordinate control methods for DG were proposed in literatures [11-20], which include the consensus synchronization control through the state feedback control [11-14], the distributed cooperative adaptive control [15, 16], the centralized proportional-integral (PI) compensation control [17-19], and the synchronization signal injection control [20]. In order to reduce the dependence on communication, the event-triggered transmission scheme [19, 21], the intermittent transmission scheme [22], and the sparse communication manner [14, 23] were proposed. Although the control accuracy is ensured under the reduced communication utilization, the possible communication failure, which may make the control methods unavailable in [11-20], drives us to consider the decentralized control manner. In order to avoid the establishment of communication links, the droop control can be improved directly. Thus, each DG only requires its own information. In previous literatures, some common decentralized control methods include the secondary control based on adaptive state estimation [24], the synchronization method through the technique of load change detection [25], the dynamic state estimation technique based on Kalman filter [26], the enhanced compensation by virtual impedance [27], and the virtual power source control technology [28]. Compared with the centralized/distributed coordinate control, the autonomy, reliability, flexibility, and scalability of MG are improved significantly in the decentralized control [21, 25].

This paper presents a new decentralized control method to realize the strict FR and accurate RPS in islanded MG. By means of changing the frequency reference (FRE), using the LVD compensation to improve the voltage droop coefficient, and adding the output voltage feedback at the voltage droop control terminal, the basic P-f droop control is improved finally. The main features are listed below:

a) Different from the virtual impedance method which introduces a relatively large virtual inductor, a virtual negative resistance is used to offset the line resistance while preventing the increase of harmonics by virtual inductor.
b) Based on the detection of active power change, the FRE is changed correspondingly for compensating the FD, which is a new real-time FR control method.
c) By the LVD compensation, the voltage droop coefficient is improved, which makes the RPS accurate under the no change in actual voltages whose difference remains. Dif-

ferent from the voltage synchronization methods in some references, the VD is unnecessary to be reduced here.

d) To ensure the RPS accuracy, the output voltage feedback control, which is rarely used in traditional voltage droop control, is proposed. The feedback reference is designed based on the desired accuracy of RPS. A low-pass filter is used to realize the feedback tracking of the reference. Notice that only the voltage satisfying the accurate RPS will be desired after the LVD compensation.

The rest of this paper is organized as follows. Considering the inverter impedance, the P-f droop control is given in section 2. Section 3 and section 4 introduce the proposed FR and RPS control methods, respectively. The simulation results of a tested MG model are shown in section 5. Finally, section 6 summarizes the paper and gives the conclusion.

## 2. P-f droop control considering the inverter impedance

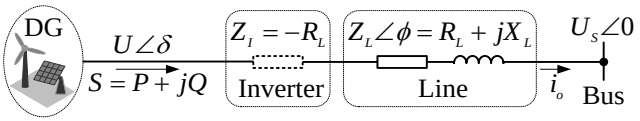


**Fig. 1.** Equivalent circuit of an inverter-connected DG.

The equivalent circuit of DG is shown in Fig. 1, where $U\angle\delta$ is the output voltage of DG, $U_S\angle 0$ is the bus voltage, $S=P+jQ$ is the output powers of DG, $i_o$ is the line current, $Z_L\angle\phi=R_L+jX_L$ is the line impedance, and $Z_I$ is the inverter impedance which is not a real physical impedance but the equivalent impedance when the current is equivalent to $i_o$. Each DG is connected to MG through an interfaced inverter. The virtual impedance method is used to set the value of inverter impedance as the given virtual impedance [29]. The output powers of DG can be expressed as:

$$\begin{cases} P=\left[U^2\cos(\phi)-UU_S\cos(\phi+\delta)\right]/Z \\ Q=\left[U^2\sin(\phi)-UU_S\sin(\phi+\delta)\right]/Z \end{cases} \tag{1}$$

Considering the output power change caused by disturbance $\Delta U$ and $\Delta\delta$ at the quiescent point $(U_e,\delta_e)$, where the power angle $\delta_e\to 0$ is very small due to the small line impedance, the small signal model of output power can be expressed as (2) after linearization.

$$\begin{cases} \Delta P=[\partial P/\partial\delta]\Delta\delta+[\partial P/\partial U]\Delta U \\ \Delta Q=[\partial Q/\partial\delta]\Delta\delta+[\partial Q/\partial U]\Delta U \end{cases} \tag{2}$$

where the powers sensitivities are expressed as:

$$\begin{cases} \partial P/\partial\delta=U_SU_e\sin(\phi+\delta_e)/Z \\ \partial P/\partial U\simeq[(2U-U_S)\cos\phi]/Z\big|_{\delta_e\simeq 0} \\ \partial Q/\partial\delta=-U_SU_e\cos(\phi+\delta_e)/Z \\ \partial Q/\partial U\simeq[(2U-U_S)\sin\phi]/Z\big|_{\delta_e\simeq 0} \end{cases} \tag{3}$$

In (3), the sensitivities or coupling intensity $\partial P/\partial U$ and $\partial Q/\partial\delta$ are large because of the very small $\phi$ in a LV MG, which means the strong coupling between active power and reactive power in the P-f droop control. The system stability may be impaired. Only if $\phi=90^\circ$, there will be $\partial P/\partial U=0$ and $\partial Q/\partial\delta=0$. As shown in Fig. 2, when $\phi=0^\circ$, that is the typical P-U droop control. When $0^\circ<\phi<90^\circ$, the change in frequency can influence the reactive power, and the change in voltage can influence the active power, which shows the powers coupling. When $\phi=90^\circ$, the reactive power is only related to frequency, and the active power is only related to voltage, which indicates the powers decoupling. Based on the impacts of line impedance angle on powers coupling, the inverter impedance is used here to modify the line impedance angle $\phi$ to $90^\circ$ (absolutely inductive line) in a LV MG.

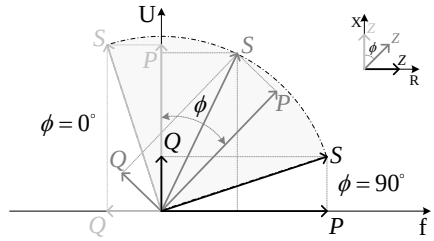


**Fig. 2.** Impacts of line impedance angle on powers coupling.

Two manners through introducing a large virtual inductance to increase the inductive proportion or a large virtual negative resistance to reduce the resistive proportion can be used. The extra inductance may result in the high frequency noise or harmonics [19]. For the above considerations, the inverter impedance is designed as follows:

$$Z_I=-R_L \tag{4}$$

By (4), the modified line impedance $Z=Z_L+Z_I=jX_L$ will be completely constituted by the line inductance. Due to $\delta\simeq 0^\circ$ and $\phi=90^\circ$, the following results are obtained:

$$\begin{cases} \cos(\phi+\delta)=-\sin\delta\simeq-\delta \\ \sin(\phi+\delta)=\cos\delta\simeq 1 \end{cases} \tag{5}$$

Substitute (5) into (1) to obtain the following equations:

$$\delta=\left(X_L/U_SU\right)\cdot P \tag{6a}$$

$$U-U_S=\left(X_L/U_S\right)\cdot Q \tag{6b}$$

From (6b), the VD between DG$i$ and DG$j$ is derived as $\Delta U=(\Delta X_L\Delta Q)/U_S$. If the inverter impedance is not considered, the VD will be $\Delta U'=(\Delta X_L\Delta Q+\Delta R_L\Delta P)/U_S$ [28]. For the given length and type of lines in a LV MG, the line resistance difference is much larger than the line inductance difference $\Delta R_L\gg\Delta X_L$, such that $\Delta U'>\Delta U$. Thus, the inaccuracy of RPS may be further expanded. Only if the generation capacities of DG$i$ and DG$j$ are the same, there will be $\Delta U'=\Delta U$ because of the always accurate active powers sharing ($\Delta P=0$) [14]. And the accuracy of RPS remains constant. The above analysis shows that the inverter impedance may also reduce the inaccuracy of RPS in some cases.

Eq. (6) can be rearranged as the P-f droop form:

$$f=f_n+mP \tag{7a}$$

$$U=U_n+nQ \tag{7b}$$

where $f_n$, $U_n$ are the references (rated value), and $m$, $n$ are the frequency, voltage droop coefficients, respectively.

$$m=(f_{\min}-f_n)/P_{\max} \tag{8a}$$

$$n=(U_{\min}-U_n)/Q_{\max} \tag{8b}$$

where $f_{\min}$, $U_{\min}$ are the minimum frequency, voltage of DG, and $P_{\max}$, $Q_{\max}$ are the maximal generation powers or the powers capacity of DG.

## 3. Proposed FR control method

The method for FR control is described here. Based on the detection of DG's active power change by wavelet transform (WT), the real-time FD is obtained. To achieve the FR, the corresponding change of reference is used to compensate the FD. And a fast restoration rate can be finally obtained by setting an exponential attenuation manner of FD.

### *3.1. Change of FRE*

The frequency droop curve is shown in Fig. 3 where line $l_o$ is the traditional droop curve which will turn into the line $l_1$ or $l_2$ when the reference is changed, $f(t)$ is the real-time frequency of DG, $P(t)$ is the real-time output active power of DG, $\Delta f(t)$ is the real-time FD, $\delta f(t)$ is the change of real-time FD, $f_n(t)$ is the real-time FRE, and $t=0$, $j-1$, $j$ are the initial, ($j$-1)th, $j$th change moments of active power, respectively. Points $o$, $a/e$, $b/c/d$ are corresponding to the moments $t=0$, $j-1$, $j$, respectively. On the line $l_o$, the frequencies of points $e$ and $d$ deviate from the rated value with $\Delta f(j-1)$ and $\Delta f(j)$ when the active power changes to $P(j-1)$ and $P(j)$ at $t=j-1$, $j$. And the FD is proportional with the active power. Therefore, a decentralized FR control method for DG is then designed.

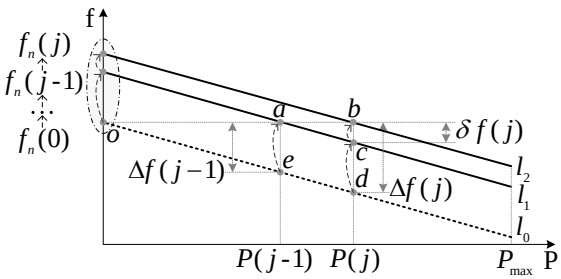


**Fig. 3.** Frequency droop characteristic curve.

The fast and reliable detection of active power change is required in the realization of FR. Because the WT can detect the instant signal change, it has been widely used in the detection of parameters change in the MG, including the powers [30]. Here, the active power is used as the input signal to the WT. A continuous WT for active power signal $P(t)$ at a scale factor $m$ and a translation factor $n$ [24] is given as:

$$W_{m,n}(t)=|m|^{-1/2}\int P(t)\psi\left((t-n)/m\right)dt \tag{9}$$

where $\psi(t)$ is the mother wavelet. The coefficients of WT, which are decomposed by $P(t)$, are given by the following inner product with $m>1$ and $n>0$.

$$C(m,n)=\int P(t)W'_{m,n}(t)dt \tag{10}$$

Although a high sampling frequency is beneficial to improving the detection accuracy, the engineering implementation is not realistic. By balancing two aspects, the sampling frequency is generally set as several thousand hertz (10kHz) [31, 32]. The continuous sampling time should be more than the frequency response time to the change and the least FR time (0.3s), which ensures an effective FR after each change. The wavelet coefficients in (10) can rapidly increase from a low value when $P(t)$ changes. If they exceed the specific threshold, the change will be detected. But a small disturbance signal in power may cause the misjudgement of system even if there are no changes in power. In order to distinguish the change signal from the disturbance signal, the threshold is set as $\pm 1\%$ of current active power, which is based on the permissible change amplitude of power disturbance. Notice that only the change in active power whose amplitude exceeds the above threshold will be detected.

Assume that there is no power demand at $t=0$ and the active power change at $t=1,\ldots,j-1,j,\ldots,n\ (j\geq 2)$. Define the matrix of active power change with $\Delta P(0)=0$ as:

$$\boldsymbol{A}=\left[\Delta P(0)\ \ \cdots\ \ \Delta P(j)\ \ \cdots\ \ \Delta P(n)\right]^T \tag{11}$$

where $\Delta P(j)=P(j)-P(j-1)$ denotes the detected value of active power change by WT at $t=j$. Then, based on (7a), the change value of FD at $t=j$ is derived as:

$$\delta f(j)=m\cdot\Delta P(j) \tag{12}$$

Define the matrix of FRE change with $\Delta f_n(0)=0$ as:

$$\boldsymbol{B}=-m\boldsymbol{A}=\left[\Delta f_n(0)\ \ \cdots\ \ \Delta f_n(j)\ \ \cdots\ \ \Delta f_n(n)\right]^T \tag{13}$$

where $\Delta f_n(j)=f_n(j)-f_n(j-1)=-\delta f(j)$ to offset $\delta f(j)$ denotes the change value of FRE at $t=j$.

Define the matrix of FREs with $f_n(0)=50\text{Hz}$ as:

$$\boldsymbol{F}=\left[f_n(0)\ \ \cdots\ \ f_n(j)\ \ \cdots\ \ f_n(n)\right]^T \tag{14}$$

Based on (11)-(14), the following nonhomogeneous linear equation (NLE) can be obtained.

$$(\boldsymbol{C}-\boldsymbol{E})\boldsymbol{F}=m\boldsymbol{A} \tag{15}$$

where $\boldsymbol{C}-\boldsymbol{E}$ is a ($n$+1)-dimensional coefficient matrix with $\text{rank}(\boldsymbol{C}-\boldsymbol{E})=n$, $\boldsymbol{E}$ is an identity matrix, and $\boldsymbol{C}$ is a constant matrix with $\text{rank}(\boldsymbol{C})=n$.

$$\boldsymbol{C}=\begin{bmatrix}1&0&\cdots&0&0\\1&0&\cdots&0&0\\0&1&\cdots&0&0\\\vdots&\vdots&\ddots&0&0\\0&0&\cdots&1&0\end{bmatrix}_{(n+1)\times(n+1)} \tag{16}$$

The changeable FRE components constitute the solution space $\boldsymbol{F}$ of above NLE. Because of a given initial condition $f_n(0)=50\text{Hz}$, $\boldsymbol{F}$ is definite (i.e. the special solution).

The real-time calibration of FRE is actually an iterative process from (11) to (14) with an initial value 50Hz. In order to avoid the one-time large amplitude of calibration, the FRE is changed in a progressive way. Due to uncertainty of loads change, it is preferential to obtain the current reference. And the real-time reference is also obtained easily under the case of continuous or frequent active power change in loads.

As shown in Fig. 3, the point $a$ on line $l_1$ and the point $b$ on line $l_2$ represent the improved droop characteristics at $t=j-1$ and $j$, respectively. The FD is added to the original reference to constitute the corresponding FREs of points $a$ and $b$. Changes of reference are reflected in the differences between point $a$ and point $e$ or between point $b$ and point $d$. When loads change at $t=j$, the FRE should be changed from $f_n(j-1)$ to $f_n(j)$. Otherwise, the FD $\delta f(j)$ exists at point $c$. Overall, different active powers correspond to different references. Through changing the FRE and offsetting the FD, the final FR within the permissible range of active power is achieved.

*3.2. Restoration rate analysis*

To analyze the rate of FR, the change of FRE is equivalent to adding a control term $\delta f_n(t)$ to the reference in (7a).

$$f = f_n(j) + mP(j) = [f_n(j-1) + \delta f_n(t)] + mP(j) \quad (17)$$

where $\delta f_n(t)$ is defined as an appropriate function which can be stabilized at $m\Delta P(j)$ in the steady state.

Define the change rate of $\delta f_n(t)$ as:

$$d\left(\delta f_n(t)\right)/dt = k \cdot \delta f(t) \quad (18)$$

where $k$ is a constant which determines the overall rate of FRE change or FR, and $\delta f(t)$ is the change value of FD. In this paper, the $\delta f_n(t)$ is used to offset the $\delta f(t)$ so that $\delta f_n(t) = -\delta f(t)$. Thus, the dynamics of FD under the above change rate are determined by the following analysis:

$$d\left(\delta f(t)\right)/dt = -d\left(\delta f_n(t)\right)/dt = -k \cdot \delta f(t) \quad (19)$$

Solve the above differential equation to obtain as:

$$\delta f(t) = c_\delta \cdot e^{-kt} \quad (20)$$

where $c_\delta$ is a constant coefficient. Eq. (20) indicates that the change of FD can be attenuated exponentially to zero at the certain rate which is determined by constant *k*. The proposed FR control system is presented in Fig. 4 where local decentralized database is used to store the active power and the FRE of DG at each change moment detected by WT.

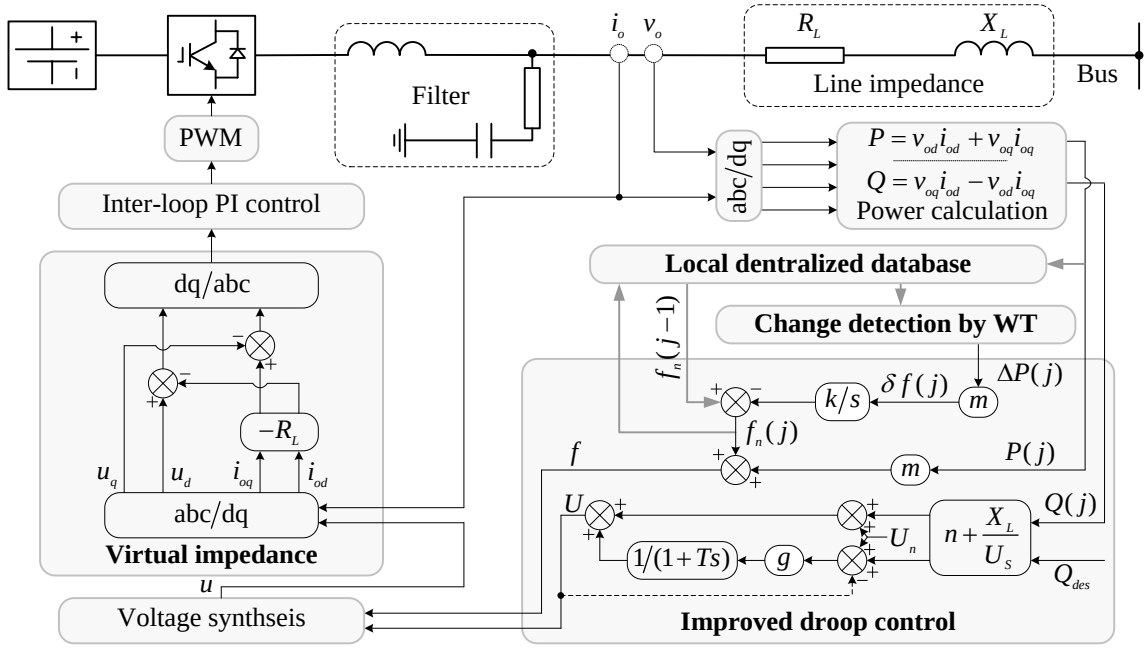


**Fig. 4.** Proposed decentralized control system of DG.

## 4. Proposed RPS control method

In this section, the solution for RPS inaccuracy is formulated. By analyzing the reason of RPS inaccuracy, the LVD compensation to increase the voltage droop coefficient can be used here. Thus, the RPS is accurate in spite of the difference in actual voltages. Besides, the output voltage feedback control through a low-pass filter is then designed. The reasonable adjustment of parameters can provide an accurate feedback tracking for output voltage.

*4.1. Description of RPS inaccuracy*

For any two parallel DGs with a common bus in the MG (e.g. DG*k*, DG*l*), they share a same bus voltage and have an equal rated voltage (i.e. $U_{Sk} = U_{Sl}$, $U_{nk} = U_{nl}$). Based on the above sample, we can substitute (6b) into (7b) to obtain the following equation as:

$$(X_{Lk}Q_k)/U_S - n_k Q_k = (X_{Ll}Q_l)/U_S - n_l Q_l \quad (21)$$

Based on (21), the proportion of RPS can be obtained as:

$$Q_k/Q_l = \left[(X_{Ll}/U_S) - n_l\right]/\left[(X_{Lk}/U_S) - n_k\right] \quad (22)$$

Form (8b), the $n_k/n_l = Q_{\max l}/Q_{\max k}$ is obtained. If their lines impedances satisfy $Z_{Lk}/Z_{Ll} \neq n_l/n_k$, the following results can be derived by (22):

$$Q_k/Q_l \neq n_l/n_k \text{ or } Q_k/Q_l \neq Q_{\max k}/Q_{\max l} \quad (23)$$

Substitute (23) into (7b) to obtain $U_k \neq U_l$, which indicates that the mismatched lines impedances can really result in the VD and inaccurate RPS.

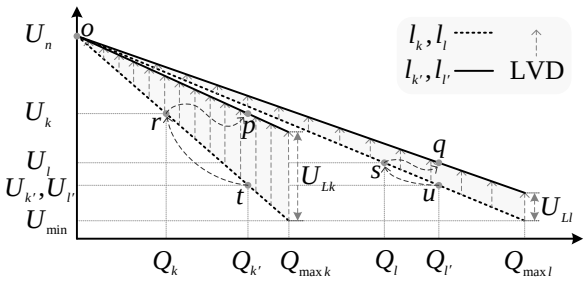


**Fig. 5.** Voltage droop characteristic curve.

The voltage droop characteristics are described in Fig. 5, where lines $l_k, l_l$ are the traditional droop curves, lines $l_{k'}, l_{l'}$ are the droop curves with LVD compensation and improved voltage droop coefficient, $U_k, U_l$ and $Q_k, Q_l$ are the actual output voltages and reactive powers, $U_{k'}, U_{l'}$ are their theoretical voltages, $Q_{k'}, Q_{l'}$ are the desired output reactive powers, $U_{Lk}, U_{Ll}$ are the LVDs, points $r/t/p$ and $s/u/q$ correspond to the actual/theoretical/modified operating statuses. If the $U_{Lk}, U_{Ll}$ are non-existent, the same $U_{k'}, U_{l'}$ will result in the accurate RPS $Q_{k'}:Q_{l'}$ at the operating points $t, u$. But, the line impedance may result in the different $U_{Lk}, U_{Ll}$. Thus, the $U_k, U_l$ are different. If lines $l_k, l_l$ are still used to control DG*k*, DG*l*, the problem of inaccurate RPS $Q_k:Q_l$ will appear at the operating points $r, s$. The LVD compensation is used here to reduce or even eliminate the above inaccuracy.

*4.2. Modified voltage droop control by LVD*

Since the VD caused by LVD is inevitable, we can raise the voltage droop characteristic by adding the LVD compensation, which can achieve the accurate RPS without worrying the VD. As shown in Fig. 5, if the modified droop lines $l_{k'}, l_{l'}$ are used to control DG*k*, DG*l*, the operating points will change from $r, s$ to $p, q$, and the corresponding RPS will be restored to $Q_{k'}, Q_{l'}$ even if $U_k \neq U_l$. The control equation of lines $l_{k'}, l_{l'}$ is obtained by adding the LVD in (6b) to traditional voltage droop control equation in (7b).

$$U = U_n + (X_L Q)/U_S + nQ = U_n + (n + X_L/U_S)Q \quad (24)$$

From (24), the droop compensation by LVD is converted to the increase in voltage droop coefficient, which reflected in Fig. 5 is the raised droop curve or the increased line slope. Substitute (6b) into (24) to obtain as:

$$U_S + (X_L/U_S)Q = U_n + (n + X_L/U_S)Q \quad (25)$$

For the DG*k* and DG*l* with $U_k \neq U_l$ controlled by (24), the following conclusions can be derived from (25).

$$Q_k/Q_l = n_l/n_k \text{ or } Q_k/Q_l = Q_{\max k}/Q_{\max l} \quad (26)$$

Eq. (26) indicates that the modified voltage droop control in (24) can really realize the accurate RPS even if the difference in actual voltages is not reduced or even eliminated.

*4.3. Output voltage feedback control*

To ensure that the voltage will be outputted after that the output reactive power has been satisfying the accurate RPS through the above improvement, the output voltage feedback control is added to the voltage control terminal. Through a low-pass filter [33], the feedback control with a desired reference is achieved. By adding the feedback term, eq. (24) of a DG (e.g. DG*i*) can be improved as:

$$U_i = U_n + \left(n_i + \frac{X_{Li}}{U_S}\right)Q_i + g_i \frac{U_{\text{des}i} - U_i}{1 + Ts} \quad (27)$$

where $g_i$ is a very small control gain, $T$ is the time constant of low-pass filter, and $U_{\text{des}i}$ is the desired voltage along with the reference in feedback loop, which is designed as (28).

$$\begin{cases} U_{\text{des}i} = U_n + \left(n_i + \dfrac{X_{Li}}{U_S}\right)Q_{\text{des}i} \\ Q_{\text{des}i} = \left[(1/n_i) \Big/ \displaystyle\sum_{o=1}^{N} 1/n_o\right] Q_l \end{cases} \quad (28)$$

In (28), $n_o$ is the voltage droop coefficient of DG, $N$ is the total number of DGs, $Q_l$ is the total reactive power demand of loads or the DGs output reactive power, and $Q_{\text{des}i}$ is the desired reactive power satisfying the accurate RPS. The additional feedback control term in (27) can make the output voltage close to the desired value (i.e. feedback reference). When the output voltage of any DG is $U_{\text{des}i}$, the $Q_{\text{des}i}$ is dispatched so that the accurate RPS is ensured. Eq. (27) can be rearranged as a standard droop form as follows:

$$U_i = (U_n + \delta U_i) + G_i(n_i + X_{Li}/U_S)Q_i \quad (29)$$

where

$$\delta U_i = \frac{g_i}{1+Ts+g_i}\left(n_i + \frac{X_{Li}}{U_S}\right)Q_{desi} \qquad (30a)$$

$$G_i = \frac{1+Ts}{1+Ts+g_i} \qquad (30b)$$

Without affecting the voltage tracking accuracy in above feedback control, the $g_i$ should be as small as possible so that $\delta U_i \simeq 0$, $G_i \simeq 1$. Thus, the final form of (29) is approximate to (24), which indicates that the adoption of feedback control hardly disturbs the voltage droop characteristic besides the objective of feedback tracking. The proposed voltage control system is also presented in Fig. 4.

## 5. Simulation

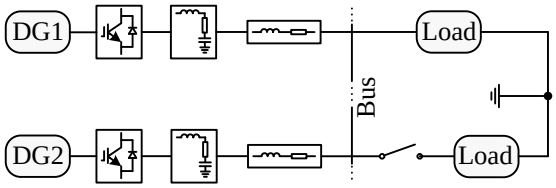


**Fig. 6.** Test MG model with two parallel DGs and several public loads.

Fig. 6 describes a typical MG model which includes two parallel DGs and public loads. Main parameters of the tested model are given in Table 1. MG operates at no-loads state (DG output powers are zero) before *t*=0s. All DGs share the total powers demand of loads equally. Performances of frequency, voltage, and reactive power are studied in four cases. To verify the effectiveness of proposed FR and RPS control methods under the loads change, the traditional control and proposed control are analyzed contrastively. The stability of above variables under a DG disturbance is also studied. Besides, the impacts of different constant *k* on FR rate and the necessity of output voltage feedback are also studied. Simulation results in RT-LAB are presented as below.

**Table 1** Main parameters of the tested MG model.

| Parameters | DG1 | DG2 |
|---|---|---|
| DC voltage | 700V | 700V |
| Filter inductance | 6mH | 6mH |
| Filter capacitance | 30μF | 30μF |
| Filter resistance | 0.2Ω | 0.2Ω |
| Line length | 1.5km | 1.0km |
| Frequency reference | 50Hz | 50Hz |
| Voltage reference | 311V | 311V |
| Frequency droop coefficient | $-2\times10^{-5}$ | $-2\times10^{-5}$ |
| Voltage droop coefficient | $-1\times10^{-3}$ | $-1\times10^{-3}$ |
| Virtual impedance | -0.963Ω | -0.642Ω |

### *5.1. Case study A: Loads change*

The case of loads change is divided into two phases: 1) increase the basal loads (1000W+3000Var) at *t*=0s; 2) increase the 100% basal loads again at *t*=1.0s. And the constant *k* is set to 250.

Performances of frequency in this case are shown in Fig. 7, where (a) is the traditional P-f droop control method and (b) is the proposed FR control method. As seen in Fig. 7(a), the FD is non-existent when the DG output active power is zero at *t*=0s. When loads is put into MG after *t*=0s, the frequency will start to deviate from 50Hz. After about an overshoot process of 0.2s, the frequency can stabilize at 49.99Hz during phase1 and 49.98Hz during phase2. The small FD is attributed to the small droop coefficient in Tab. 1. Generally, the FD is large than the above value. The above result shows that the FD is existent in the traditional droop control as long as there is change of active power, and the relation between them is proportional. When the proposed FR control method is used, the performance of FR is given in Fig. 7(b). Whether during phase1 or phase2, the frequency is restored to 50Hz, which is compensated by the change of FRE. Notice that the large overshoot amplitude is actually not an oscillation but a reflection of change in FRE. The restoration time during two phases is about 0.1s under *k*=250. The contrastive results can indicate that the proposed FR control method is effective.

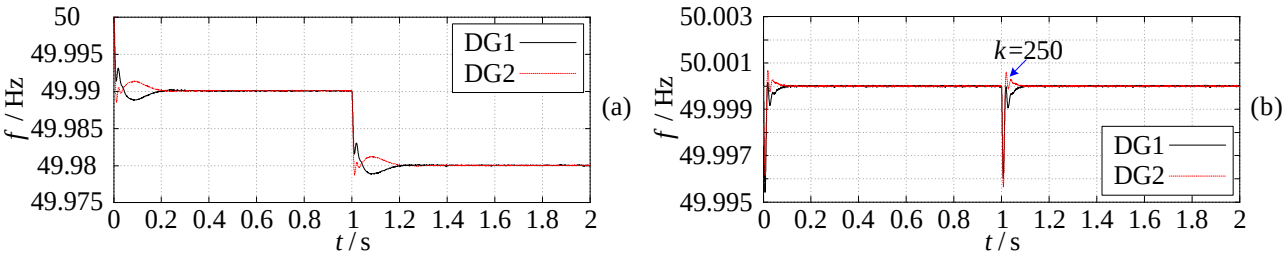


**Fig. 7.** Performances of frequency in case of loads change.

Performances of voltage and RPS in this case are given in Fig. 8, where (a)/(c) are the traditional droop control and (b)/(d) are the proposed RPS control. In Figs. 8(a) and 8(b), the voltage reduces with the increase of reactive power due to the droop characteristics. However, the unequal lines impedances result in that the VDs of 0.25V and 0.5V are existent during phase1 and phase2, respectively. In the traditional droop control, the inaccuracy of RPS is accompanied by the VD, as shown in Fig. 8(c). The steady-state sharing errors are approximate to 250Var during phase1 and 500Var during phase2. And the maximum RPS errors are about 300Var and 600Var during overshoot phases 0s~0.2s and 1s~1.2s, respectively. Besides, the total output reactive power of DGs is less than the loads demand, so that partial loads may not operate normally. In the proposed RPS control, each DG can share the reactive power of 1500Var equally in Fig. 8(d) even if the VD is not reduced or even eliminated in Fig. 8(b). The reactive power curves are almost identical and the maximum instant RPS errors are less than 100Var during overshoot phases 0s~0.1s and 1s~1.1s, respectively. This is because the application of output voltage feedback, the voltage can be outputted directly. The above contrastive results can indicate that the proposed RPS control method is effective, and the output voltage feedback can guarantee the strict RPS accuracy.

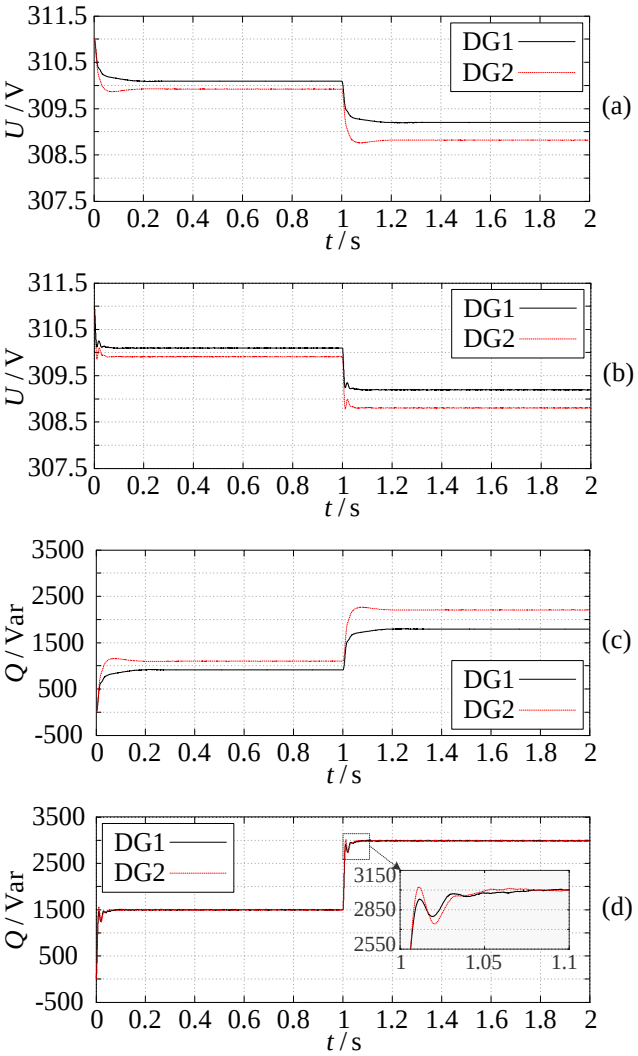


**Fig. 8.** Performances of voltage and reactive power in case of loads change.

### *5.2. Case study B: Small-instant DG disturbance*

Under the same loads change and constant $k$ with case A, a small-instant DG disturbance signal is injected into MG at $t$=1.0s. Corresponding simulation results of proposed method are shown in Fig. 9. As shown in Fig. 9(a), the frequency is still

restored quickly within 0.1s. Compared with Fig. 7(b), the main difference is reflected in the instant amplitude fluctuation caused by the sudden disturbance during overshoot phase 1s~1.1s. Impacts of disturbance on the steady-state FR and restoration rate are almost invisible. Compared with Fig. 8(b), the DG voltage still takes only 0.1s to restore the stability even if the instant voltage fluctuation of 1.3V exists in Fig. 9(b). Besides, in Fig. 9(c), the constant RPS accuracy during the steady-state phase 1.1s~2s can be attributed to the above voltage performance. The maximum RPS error caused by the disturbance is about 150Var during 1s~1.1s, which is only more 50Var than the value in Fig. 8(d). So, the steady-state RPS accuracy is also almost unaffected by the disturbance. Form the above results, it is known that the proposed method can ensure the accuracies of FR and RPS with good stability under a sudden DG disturbance.

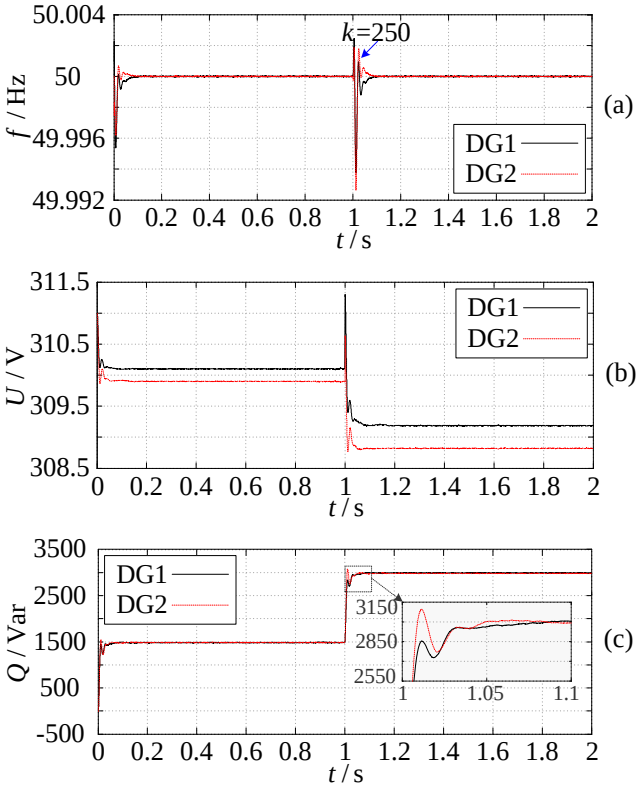


**Fig. 9.** Performances of frequency, voltage, and reactive power in proposed method in case of small-instant DG disturbance.

### *5.3. Case study C: Different constant k*

Under the same loads change with case A, performances of FR rate with different constant $k$=50 and $k$=1250 are given in Figs. 10(a) and 10(b), respectively. Compared with the restoration time of 0.1s under $k$=250 in Fig. 7(b), the FR slows down with longer adjustment time of 0.2s in Fig. 10(a), and the FR is faster with shorter adjustment time of 0.05s in Fig. 10(b). Although the FR rate changes, all restorations processes are accomplished within a relatively short time 0.2s, and the steady-state FR remains accurate. The above results indicate that the FR rate is indeed proportional to the constant $k$. Thus, we can choose a large $k$ within allowable conditions as long as the final FR accuracy is unaffected in the actual MG application.

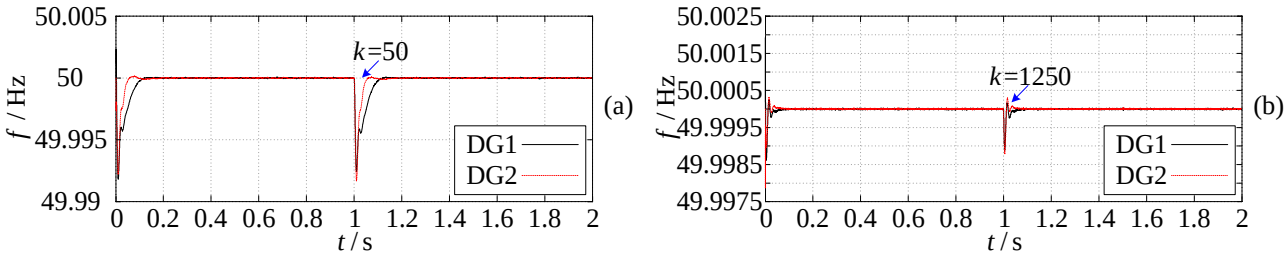


**Fig. 10.** FR rate in proposed method in case of different constant $k$.

### *5.4. Case study D: Necessity of output voltage feedback*

Under the same loads change with case A, the simulation results to show the importance of output voltage feedback in proposed method are given in Fig. 11. In Fig. 11(b), there is an obvious difference between DGs' reactive powers during 0s~0.2s and 1s~1.2s, and the maximum RPS errors may exceed 500Var that is far larger than the RPS errors of 100Var in Fig. 8(d). In Fig. 11(a), the corresponding DG voltage is still outputted even through a large RPS error exists. Relative to the consistent overshoot waveforms and short overshoot time in Fig. 8(b), the voltage characteristics influenced by the output feedback are

almost non-existent in Fig. 11(a), which is identical to Fig. 8(a). It indicates that the output voltage feedback is necessary especially for the strict adjustment of RPS during overshoot phases.

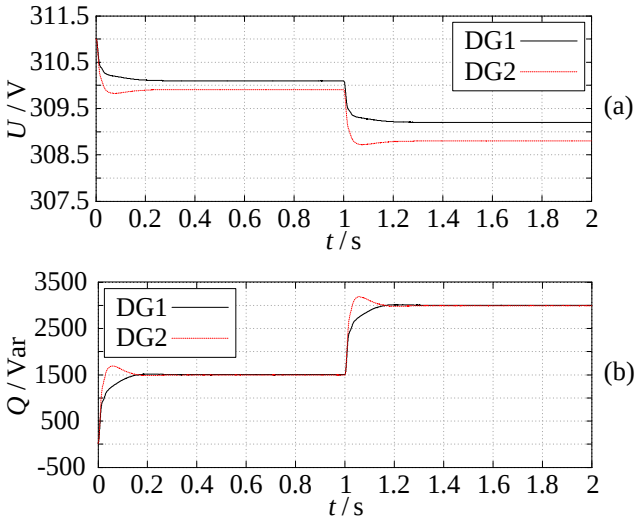


**Fig. 11.** Performances of voltage and reactive power in proposed method without output voltage feedback.

## 6. Conclusion

This paper presents an improved droop control method for FR and accurate RPS in islanded MGs. The proposed method, which only needs to modify the droop control parameters in accordance with the respective local information of each DG, is absolutely decentralized. So, no communication is required, which enhances the system reliability. The simulation results are consistent with the following facts as:

a) FR is achieved through the compensation by the change of FRE. The FR rate is improved by a large constant *k*.
b) Accurate RPS is realized by using the LVD droop compensation and the output voltage feedback which ensures the strict RPS adjustment during overshoot phases
c) The proposed method is still effective with a good stability under DG disturbance.

Based on the same principle with proposed method, the relevant FR and RPS control methods in the high-voltage or medium-voltage MG are topics for future research.

## 7. Acknowledgments

This work is supported by the National Natural Science Foundation of China under Grants 61573300, 61533010, the Hebei Provincial Natural Science Foundation under Grant E2016203374, the Jiangsu Provincial Natural Science Foundation under Grant BK20171445, and the 2017 Green Seedling Plan by Beijing Green Future Environment Foundation.

## 8. References

[1] D.E. Olivares., A.M. Sani., A.H. Etemadi., *et al*.: 'Trends in microgrid control', *IEEE Trans. Smart Grid*., 2014, 5, (4), pp. 1905-1919
[2] Z. Liu., C. Su., H.K. Hoidalen., *et al*.: 'A multi-agent system based protection and control scheme for distribution system with distributed-generation integration', *IEEE Trans. Power Del*., 2017, 32, (1), pp. 536-545
[3] T. Wu., Z. Liu., J. Liu., *et al*.: 'A unified virtual power decoupling method for droop-controlled parallel inverters in microgrids', *IEEE Trans. Power Electron*., 2016, 31, (8), pp. 5587-5603
[4] F. Shahnia., A. Ghosh.: 'Coupling of neighbouring low voltage residential distribution feeders for voltage profile improvement using power electronics converters', *IET Renew. Power Gener*., 2016, 10, (2), pp. 535-547
[5] X. Tang., X. Hu., N. Li., *et al*.: 'A novel frequency and voltage control method for islanded based on multienergy strorages', *IEEE Trans. Smart Grid*., 2016, 7, (1), pp. 410-419.
[6] H. Shi., F. Zhuo., H. Yi., *et al*.: 'A novel real-time voltage and frequency compensation strategy for photovoltaic-based microgrid', *IEEE Trans. Ind. Electron*., 2015, 62, (6), pp. 3545-3556
[7] L.D. Marinovici., J. Lian., K. Kalsi., *et al*.: 'Distributed hierarchical control architecture for transient dynamics improvement in power systems', *IEEE Trans. Power Syst*., 2013, 28, (3), pp. 3065-3074
[8] J. Li., F. Li., X. Li., *et al*.: 'S-shaped droop control method with secondary frequency characteristics for inverters in microgrid', *IET Gener. Transm. Distrib*., 2016, 10, (13), pp. 3385-3392
[9] Z. Peng., J. Wang., D. Bi., *et al*.: 'The application of microgrids based on droop control with coupling compensation and inertia', *IEEE Trans. Sustain. Energy*., 2018, 9, (3), pp. 1157-1168
[10] Y. Han., P. Shen., X. Zhao., *et al*.: 'An enhanced power sharing scheme for voltage unbalance and harmonics compensation in an islanded AC microgrid', *IEEE Trans. Energy Convers*., 2016, 31, (3), pp. 1037-1050
[11] F. Guo., C. Wen., J. Mao., *et al*.: 'Distributed secondary voltage and frequency restoration control of droop-controlled inverter-based microgrids', *IEEE Trans. Ind. Electron*., 2015, 62, (7), pp. 4355-4364
[12] S. Zuo., A. Davoudi., Y. Song., *et al*.: 'Distributed finite-time voltage and frequency restoration in islanded AC microgrids', *IEEE Trans. Ind. Electron*., 2016, 63, (10), pp. 5988-5997

[13] C. Dou., Z. Zhang., D. Yue., *et al*.: 'MAS-based hierarchical distributed coordinate control strategy of virtual power source voltage in low-voltage microgrid', *IEEE Access*., 2017, 5, (1), pp. 11381-11390

[14] N.M. Dehkordi., N. Sadati., M. Hamzeh.: 'Distributed robust finite-time secondary voltage and frequency control of islanded microgrids', *IEEE Trans. Power Syst*., 2017, 32, (5), pp. 3648-3659

[15] N.M. Dehkordi., N. Sadati., M. Hamzeh.: 'Fully distributed cooperative secondary frequency and voltage control of islanded microgrids', *IEEE Trans. Energy Convers*., 2017, 32, (2), pp. 675-685

[16] D.O. Amoateng., M.A. Hosani., M.S. Elmoursi., *et al*.: 'Adaptive voltage and frequency control of islanded multi-microgrids', *IEEE Trans. Power Syst*., 2018, 33, (4), pp. 4454-4465

[17] Q. Shafiee., J.M. Guerrero., J.C. Vasquez.: 'Distributed secondary control for islanded microgrids-a novel approach', *IEEE Trans. Power Electron*., 2014, 29, (2), pp. 1018-1031

[18] U. Sowmmiya., U. Govindarajan.: 'Control and power transfer operation of WRIG-based WECS in a hybrid AC/DC microgrid', *IET Renew. Power Gener*., 2018, 12, (3), pp. 359-373

[19] Z. Zhang., C. Dou., D. Yue., *et al*.: 'An event-triggered secondary control strategy with network delay in islanded microgrids', *IEEE Syst. J*., DOI: 10.1109/JSYST.2018.2832065

[20] J. He., Y. Li.: 'An enhanced microgrid load demand sharing strategy', *IEEE Trans. Power Electron*., 2012, 27, (9), pp. 3984-3995

[21] Y. Fan., G. Hu., M. Egerstedt.: 'Distributed reactive power sharing control for microgrids with event-triggered communication', *IEEE Trans. Control Syst. Technol*., 2017, 25, (1), pp. 118-128

[22] X. Lu., J. Lai., X. Yu., *et al*.: 'Distributed coordination of islanded microgrid clusters using a two-layer intermittent communication network', *IEEE Trans. Ind. Informat*., DOI: 10.1109/TII.2017.2783334.

[23] X. Wu., C. Shen., R. Iravani.: 'A distributed, cooperative frequency and voltage control for microgrids', *IEEE Trans. Smart Grid*., 2018, 9, (4), pp. 2764-2776

[24] G. Lou., W. Gu., L. Wang., *et al*.: 'Decentralised secondary voltage and frequency control scheme for islanded microgrid based on adaptive state estimator', *IET Gener. Transm. Distrib*., 2017, 11, (15), pp. 3683-3693

[25] M. Kosari., S.H. Hosseinian.: 'Decentralized reactive power sharing and frequency restoration in islanded microgrid', *IEEE Trans. Power Syst*., 2017, 32, (4), pp. 2901-2912

[26] S. Yu., L. Zhang., H.H.C. Lu., *et al*.: 'A DSE-based power system frequency restoration strategy for PV-integrated power systems considering solar irradiance variations', *IEEE Trans. Ind. Informat*., 2017, 13, (5), pp. 2511-2518

[27] Y. Zhu., F. Zhuo., F. Wang., *et al*.: 'A virtual impedance optimization method for reactive power sharing in networked microgrid', *IEEE Trans. Power Electron*., 2016, 31, (4), pp. 2890-2904

[28] C. Dou., Z. Zhang., D. Yue., *et al*.: 'Improved droop control based on virtual impedance and virtual power source in low-voltage microgrid', *IET Gener. Transm. Distrib*., 2017, 11, (4), pp. 1046-1054

[29] P. Sreekumar., V. Khadkikar.: 'Direct control of the inverter impedance to achieve controllable harmonic sharing in the islanded microgrid', *IEEE Trans. Ind. Electron*., 2017, 64, (1), pp. 827-837

[30] P.K. Ray, N. Kishor, S.R. Mohanty.: 'Islanding and power quality disturbance detection in grid-connected hybrid power system using wavelet and S-transform', *IEEE Trans. Smart Grid*., 2012, 3, (3), pp. 1082-1094

[31] N.W.A. Lidula., A.D. Rajapakse.: 'A pattern-recognition approach for detecting power islands using transient signals-part I: design and implementation', *IEEE Trans. Power Del*., 2010, 25, (4), pp. 3070-3077

[32] N.W.A. Lidula., A.D. Rajapakse.: 'A pattern-recognition approach for detecting power islands using transient signals-part II: performance evaluation', *IEEE Trans. Power Del*., 2012, 27, (3), pp. 1071-1080

[33] H. Xin., R. Zhao., L. Zhang., *et al*.: 'A decentralized hierarchical control structure and self-optimizing control strategy for f-P type DGs in islanded microgrids', *IEEE Trans. Smart Grid*., 2017, 7, (1), pp. 3-5